United States Department of the Interior

Geological Survey

NEAR-SURFACE HEAT FLOW IN SALINE VALLEY, CALIFORNIA

by

Charles W. Mase, S. P. Galanis, Jr., and Robert J. Munroe

Open-File Report 79-1136

1979

This report is preliminary and has not been edited or reviewed for conformity with Geological Survey standards and nomenclature.

Table of Contents

Figures

Tables

ABSTRACT

With the exception of values from one borehole drilled at Palm Spring and three boreholes drilled around Saline Valley dry lake, eight new heat-flow values in Saline Valley, California, are within or somewhat below the range one would expect for this region of the Basin and Range heat-flow province. The lack of recent volcanism in the area and the apparently normal Basin and Range heat flow suggest that geothermal systems within the valley are stable stationary phases supported by high regional heat flow and forced convection.

INTRODUCTION

Saline Valley lies along a NNW-trending series of hydrothermal convective systems stretching from the Salton Sea area along the eastern margin of the Sierra Nevada as far northward as the Modoc Plateau (Renner and others, 1975; Grim, 1977). High temperature geothermal systems near the Sierra Nevada front such as Coso and Long Valley are related to large, young volcanic features. The lack of recent volcanism in the Saline Valley area suggests that geothermal systems within the valley may be the result of deep circulation of ground water, storage, and heating within a reservoir due to a high regional heat flow with subsequent discharge to the surface through permeable fracture zones.

The present work was undertaken to provide background information for geothermal resource assessment of the Saline Valley. We have combined the results from ten holes drilled by the U.S. Geological Survey with data from an additional borehole drilled by private concerns in an attempt to determine the thermal state of Saline Valley. The following symbols and units are used frequently in the remainder of this report:

T, temperature, °C

Γ, vertical temperature gradient, $°K\ km^{-1}$ or $°C\ km^{-1}$

K, thermal conductivity, 1 $W\ m^{-1}\ °K^{-1}$ = 2.39 tcu

(1 tcu = 1 $mcal\ cm^{-1}\ s^{-1}\ °C^{-1}$)

q, heat flow, 1 mWm^{-2} = .0239 hfu (1 hfu = 1 $\mu cal\ cm^{-2}\ s^{-1}$)

In addition to latitude and longitude, the USGS Water Resources Division convention is used to specify site locations, i.e., 32/38-26bba represents NE 1/4, NW 1/4, NW 1/4, T32N, R38E, sec. 26.

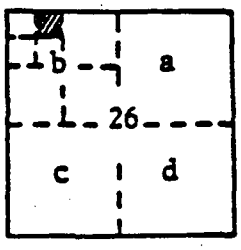

Acknowledgments: John Sass assisted by providing helpful suggestions during the data reduction and interpretation phase of the report and by providing thoughtful comments on our manuscript. Jack Porter supervised the drilling operations and temperature logging of the boreholes. Eugene Smith performed the needle-probe conductivities on the core.

GEOLOGY - HYDROLOGY

Saline Valley occupies a position near the western margin of the Basin and Range physiographic province. It is an alluvial filled intermontane valley bounded on the south and west by the Inyo Mountains and to the north and east by the Saline and Last Chance Ranges. The region is characterized by roughly parallel mountain ranges and basins having a northwesterly trend. Northward-trending geomorphic features are less obvious than in the more typical Basin and Range province to the north and east. A general geologic map of the Saline Valley area is illustrated in Figure 1. The geologic information in this figure is largely taken from Jennings (1958, 1977) and Ross (1967).

The ranges surrounding Saline Valley are comprised of strongly folded and faulted sedimentary rocks ranging in age from Cambrian to Triassic. Except for the upper part of the Triassic, these rocks are largely of marine origin and include limestone, dolomite, quartzite, and shale. These rocks were intruded extensively during the Jurrasic and Cretaceous by granitic magmas. The largest of these intrusions is the Hunter Mountain batholith which comprises nearly half of the Inyo Mountains and is related to the larger Sierra Nevada batholith to the west (Ross, 1969). Extensive basalt flows cover the main part of the Saline Range and are underlain by a sequence of rhyolite ignimbrites. These rocks are late Pliocene in age (Ross, 1970) and represent the youngest volcanism in the area; therefore, they are too old to represent heat sources for modern activity. Valley fill includes late Tertiary and Quaternary alluvial and lacustrine sediments.

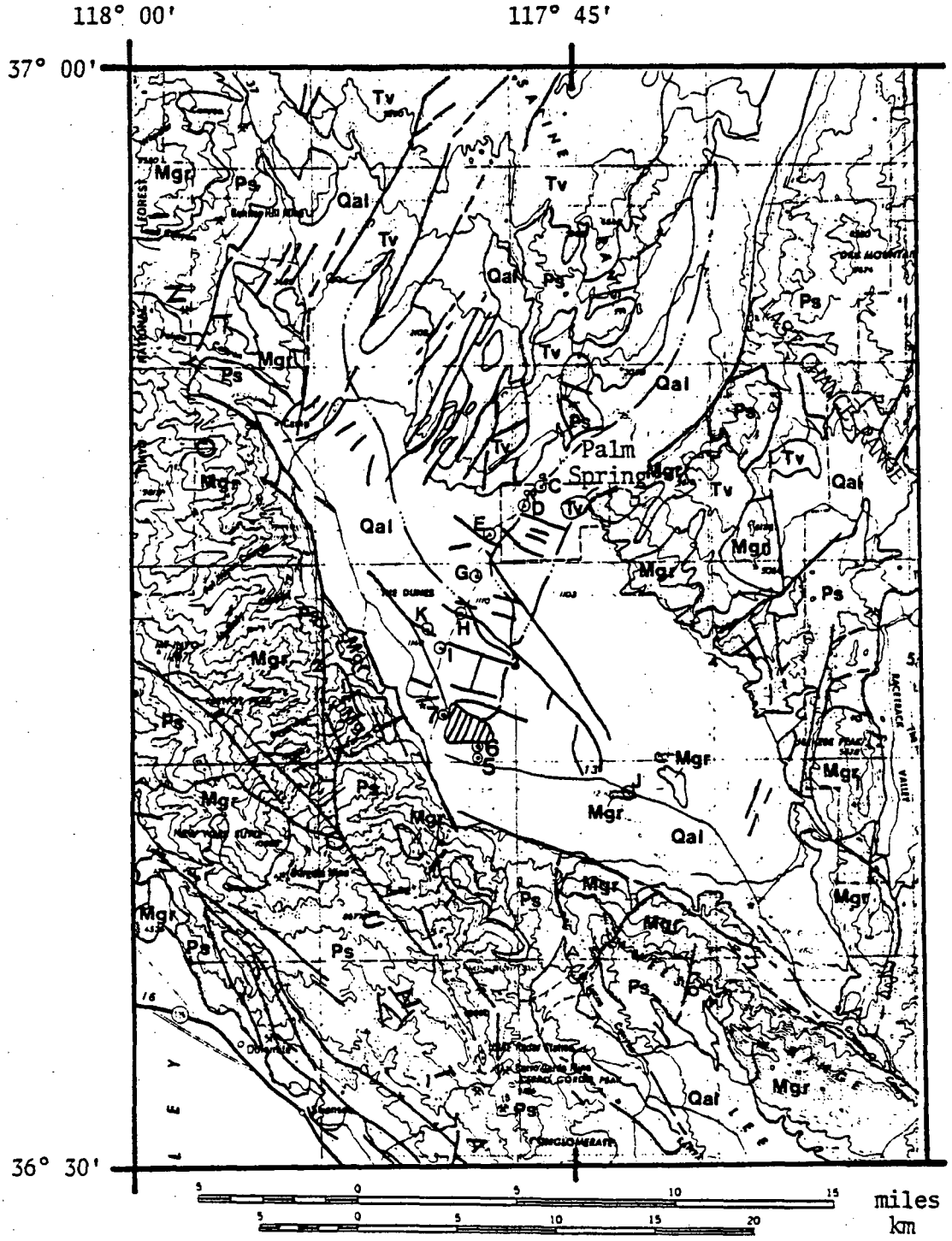

Qal - Quaternary Alluvium. Includes fan, lacustrine, eolian and calcareous tufa deposits.

Tv - Tertiary Volcanics. Predominantly Pliocene basalt.

Mgr - Mesozoic Granitics. Composed primarily of granodiorite and quartz monzonite.

Ps - Paleozoic sedimentary rocks. Includes limestone, dolomite, shale, and quartzite.

Figure 1. Geologic sketch map of Saline Valley. KGRA is outlined by dashed line. Geology and faults generalized from Jennings (1958, 1977).

The chief surface geothermal manifestation occurs at Palm Spring (Figure 1) located along the eastern margin of Saline Valley. The spring has a net discharge of 20 liters per minute at approximately 40°C (Waring, 1965). Associated with Palm Spring are the upper and lower warm springs for which no discharge rates or temperatures have been recorded. The lack of recent volcanism in the area and the association of the springs with major faults suggests that the springs are a stable stationary phase supported by a high regional heat flow and forced convection (see discussion by Lachenbruch and Sass, 1977; Kilty and others, 1978).

Regional temperature and heat-flow data obtained in Saline Valley are strongly influenced by the hydrologic system. An understanding of this data requires at least a gross understanding of the convective processes at work within the valley. For the purposes of the present study, it is appropriate to consider the hydrologic system in Saline Valley as comprising two parts: 1) a shallow subsystem in which groundwater paths are relatively short and direct, controlled by local topography and surface drainage patterns with temperatures not much higher than ambient surface temperatures, and 2) a deeper subsystem in which groundwater paths are relatively long and circuitous, governed by the configuration of fractures and permeable formations and forced by a regional piezometric gradient controlled by topography and precipitation with temperatures commonly much higher than ambient surface temperature. The valley fill of the shallow subsystem is composed of unconsolidated lacustrine and fan deposits of gravel, sand, silt, and clay. This heterogeneous composition causes the permeability of the fill to vary from good to poor and forms clayey layers which separate shallow aquifers within the valley fill.

These clayey layers probably also serve to separate the shallow and deep subsystem except locally where fault and fracture zones with large effective permeabilities provide interconnecting conduits for upward and downward ground water flow.

Recharge to sedimentary aquifers in the deep subsystem occurs in the mountainous areas which receive 100-300 mm of water per year as precipitation. The aquifers can recharge directly from infiltration of precipitation and runoff wherever they outcrop, otherwise their recharge depends upon the configuration of fractures and permeable formations in the overlying rock. The recharge of sedimentary aquifers in the shallow subsystem is derived from infiltration of precipitation and runoff from the surrounding mountains.

GEOTHERMAL GRADIENT DATA

To provide background information for a geothermal resource assessment of Saline Valley, a series of ten geothermal gradient - heat flow boreholes was drilled by the U.S. Geological Survey. The results from these boreholes are combined with data from an additional borehole (SVK) in an attempt to understand the thermal state of the valley. Temperature and detailed conductivity measurements were made on each borehole (except for SO5, SO6, SO7, and SVK) to provide estimates of conductive heat flow. Figure 1 shows the location of the boreholes, and Figure 2 illustrates the temperature-depth curves for the Saline Valley holes.

Below the zone of seasonal variation, boreholes SO5 and SO6 (Figures 11 and 12) show a strong consistent upward curvature characteristic of areas in which downward water movement is taking place. SO7 (Figure 13) also exhibits numerous water flow disturbances indicative of both lateral and vertical ground water movements within the valley fill. SO5, SO6, and SO7 are located along the edge of an intermittent lake that occupies the central depression of Saline Valley. The temperature-depth curves for these boreholes suggests that the lowland area is a zone of hydrologic recharge for shallow aquifers contained within the valley fill in which the circulation of relatively cold ground water is masking deeper thermal activity.

Water was flowing slowly but steadily from the collar of SVK. Examination of the temperature profile (Figure 10) indicates a local upflow of water from approximately 80 m to the surface. However, no vertical water movement is indicated below the influx of artesian flow and the temperature profile below this point is linear and consistent with those from SVH and SVI (Figure 2). SVK was originally drilled for purposes other than heat flow. As a result no

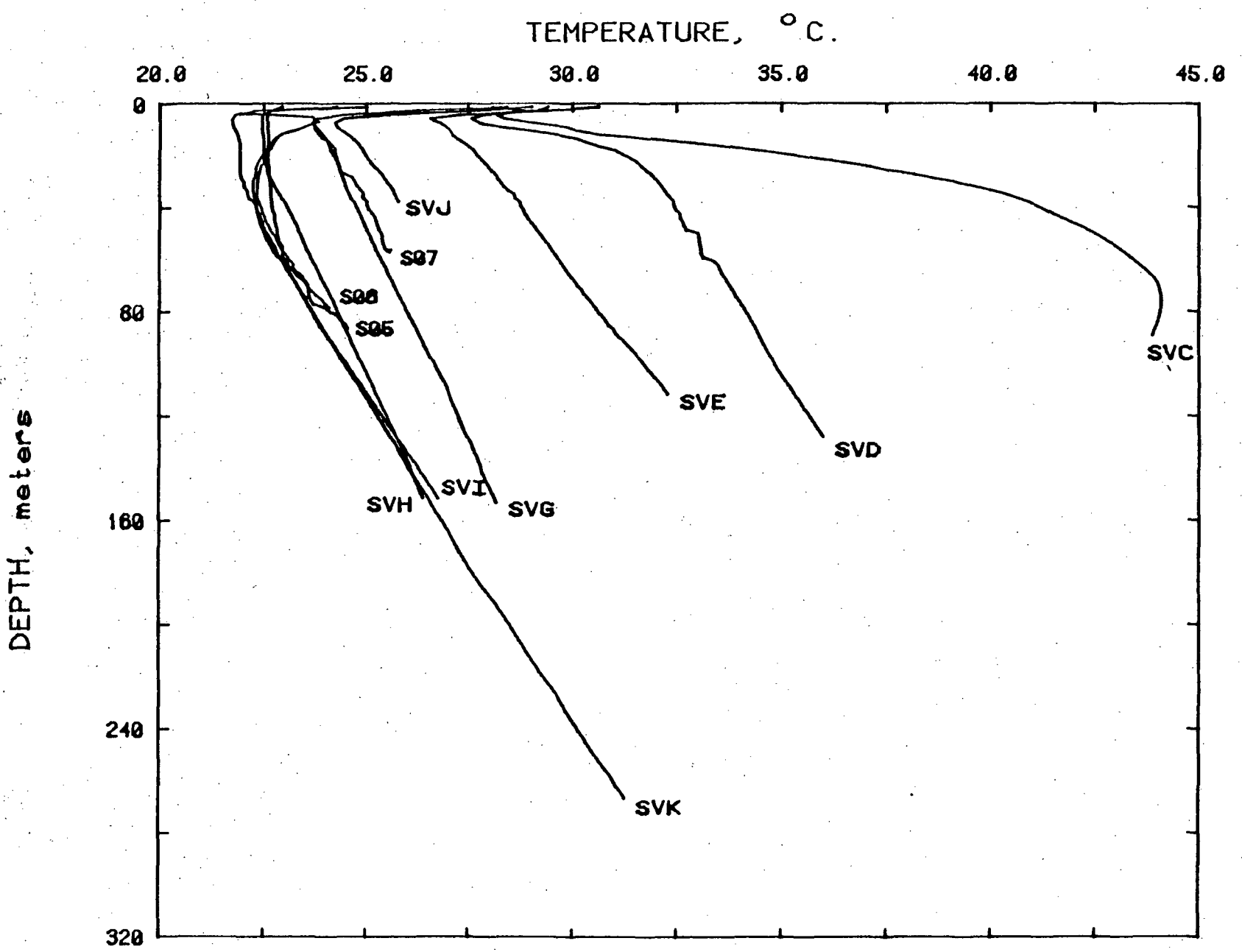

Figure 2. Temperature-depth curves, Saline Valley, California.

drill cuttings were available to measure thermal conductivities, and only a temperature log was obtained for the borehole. The thermal conductivity used for calculating the heat flow listed for SVK in Table 1 was estimated by averaging the conductivity determinations for SVH and SVI which are judged to be representative of the rock types in SVK.

Borehole SVD has a local water-flow disturbance from approximately 49 m to 61 m (Figures 2 and 4). Above this zone, the profile exhibits a consistent, downward curvature. The presence of warm springs located midway between SVD and Palm Spring is interpreted as indicating lateral movement of thermal fluids within the near-surface alluvial gravels. Thus the high surface temperature, water-flow disturbance and curvature displayed by SVD may be attributed to a combination of diffused upward convection around the borehole and lateral migration of thermal fluids westward from Palm Spring into the alluvium. Below 61 m the temperature profile is quite linear with a gradient of 38°C km^{-1} indicating heat transfer is primarily accomplished by conduction. The change in gradient at approximately 104 m is due to a thermal conductivity change within the alluvium. The relatively high gradient and surface temperature exhibited by SVE (Figure 5) may also be attributed to the leakage of thermal fluids westward into the valley fill from Palm Spring.

The nearly isothermal appearance and reversal of the bottom of the profile from Palm Spring, SVC, (Figures 2 and 3) indicates that water discharged at or near the surface in the hot spring is moving laterally in the alluvium overriding colder ground water. A peculiarity of temperature-depth curves near strongly convecting zones is that the thermal gradient is large and quite variable with depth so that making extrapolations on the basis of this curve is risky. However, the discharge temperature of 40°C (Waring, 1965)

and maximum measured temperature of 44°C (Figure 3) suggests that the central portion of the Palm Spring system is isothermal at 44°C to depths of 100 m. An upward ground water flow from a reasonably shallow depth of approximately 1 km can maintain the maximum observed temperatures at Palm Spring. The remaining boreholes (SVG, SVH, SVI, and SVJ) show linear profiles with gradients ranging from 30 to 49 °C km^{-1} (Figure 2) in which heat transfer seems to be exclusively by conduction. However, the variation in surface temperatures for these closely spaced boreholes suggests that weak, diffused ground water movements within the valley fill may partially mask the heat flow associated with conditions at depth.

HEAT FLOW

The vertical component of heat flow, q, was computed as the product of the harmonic mean thermal conductivity, K, and the least-squares temperature gradient, Γ, over each linear section of the temperature profile. Thermal conductivities were measured on core with a variant of the needle-probe method (Von Herzen and Maxwell, 1959) or from drill chips in a divided-bar apparatus following the methods described by Sass and others (1971a, 1971b). Assigning a single gradient to boreholes exhibiting curvature in the temperature-depth plot such as SVC, for the purposes of calculating a conductive heat loss is somewhat arbitrary. In general, the most linear section of the near-surface temperature-depth curve was used to calculate the least-squares gradient. Table 1 gives results for each hole including the harmonic mean thermal conductivity, the depth interval and corresponding gradient, heat flow, and an estimate of the standard error residing in each value.

The value of 780 mW m^{-2} listed for the borehole at Palm Spring (SVC) is the heat flow through the conductive cap of the geothermal system. Since geothermal systems have large and locally variable temperature gradients, we may expect the heat flow to vary dramatically in the vicinity of the spring. Therefore the value of 780 mW m^{-2} should only be taken as a very localized value of conductive heat flux. We may also expect this value to decrease dramatically as we move laterally away from the spring as indicated by the value of 67 mW m^{-2} recorded at SVD 1 km southwest of the hot spring.

Estimation of the power loss for a geothermal system yields insight into the nature and origins of the thermal fluids and sources. The power loss at

TABLE 1. Heat-flow calculations for Saline Valley

Well #	Designation	N. Lat.	W. Long.	Elev m	Depth range m	N	K		Γ		q	
							$W\ m^{-1}\ °K^{-1}$ tcu	(SE)* (SE)*	°K km^{-1}	(SE)*	$mW\ m^{-2}$ hfu	(SE)* (SE)*
SVC	13S/39E-18dac	36° 48.4'	117° 46.1'	427	14-35	1	2.00 4.78	(.15) (.36)	390.1	(12.8)	781 18.7	(71)** (1.7)**
SVD	13S/39E-19bcb	36° 47.9'	117° 46.9'	400	49-128	7	1.78 4.23	(.13) (.31)	37.87	(.25)	67 1.60	(5) (.13)
SVE	13S/39E-25bbd	37° 47.2'	117° 47.9'	357	18-112	6	1.77 4.23	(.13) (.31)	48.96	(.23)	87 2.08	(7) (.15)
SVG	13S/38E-35aca	36° 46.2'	117° 48.4'	341	13-153	13	1.70 4.06	(.13) (.30)	30.64	(.10)	52 1.24	(4) (.10)
SVH	14S/38E-2cba	36° 45.4'	117° 48.9'	334	27-152	13	1.75 4.18	(.13) (.31)	30.43	(.08)	53 1.27	(4) (.10)
SVI	14S/R38-10dac	36° 44.2'	117° 49.5'	330	50-152	13	1.68 4.01	(.13) (.30)	42.53	(.13)	72 1.71	(5) (.13)
SVJ	15S/39E-3bba	36° 42.5'	117° 42.5'	354	13-38	2	1.51 3.61	(.09) (.22)	46.94	(.87)	71 1.69	(5) (.12)
SVK	14S/38E-10baa	36° 44.5'	117° 49.7'	332	80-267	0	1.69 4.04	(.12) (.29)	40.38	(.05)	68 1.63	(5) (.12)

*SE represents standard error

**Heat flux through conductive cap of Palm Spring thermal system

Palm Spring may be estimated by integrating the conductive heat flow over the system and adding to this the enthalpy of the discharge waters. For the purposes of calculating a conductive heat loss, we arbitrarily define the "system" to be circular in plan with decreasing heat flow radially outward from the spring and an outer boundary near SVD. Our definition results in an area of 7 km^2 for the system. There is some justification for this when we examine detailed heat-flow patterns for similar Basin and Range hydrothermal systems like Leach Hot Springs, Nevada (Sass and others, 1977), Gerlach KGRA, Nevada (Olmsted and others, 1975; Sass and others, 1979), and Newcastle, Utah (Rush, personal communication); all of which are roughly circular in plan. The anomalous conductive heat loss is roughly 2 MW. The discharge at Palm Spring is 20 liters per minute (Waring, 1965) at a temperature of 40°C. This yields a convective power loss of .03 MW. A coarse estimate of the heat discharge from Palm Spring is thus 2 MW. If the anomalous heat discharge is supported entirely by the enthalpy of the thermal waters, then a minimum mass discharge of 20 kg sec^{-1} at 44°C is required of the system. For this mass discharge rate 0.3 kg sec^{-1} is vented at the surface in the form of Palm Spring, the remainder is discharged into shallow aquifers within the alluvium with the heat being lost through a conductive cap as illustrated by borehole SVC. Presuming that the upward flow takes place over the central portion of the system (approximately 10^5 m^2), the vertical ground water velocity through the permeable zone may be estimated as 2×10^{-7} m sec^{-1} (6 m yr^{-1}). The permeability of the fault zone through which the fluids rise is not known. However, if we consider an average value of 5 darcies (Sorey, 1975) for the permeable part of the fault zone, a vertical piezometric gradient of less than 1% is required to account for the discharge. This is equivalent to a

10 m decrease in piezometric head in a 1 km rise from the reservoir to the surface.

The net heat discharge at Palm Spring is equivalent to the normal Basin and Range heat flow over 25 km^2. If we assume that the heat discharge in the vicinity of the spring is balanced by recharge in other parts of the system and that recharging ground water absorbs 30% to 50% of the regional heat flow as is the case for the Roosevelt hot springs region, Utah (Ward and others, 1978), heat absorbed over a recharge area of 50 to 85 km^2 could maintain the observed power loss. Supposing that the ground water percolates downward uniformly, then vertical ground water velocities in the recharge zone required to sustain the discharge rate at Palm Spring range from 8 to 13 $mm\ yr^{-1}$ (30% and 50% heat absorption, respectively), some 5% to 10% of the local annual precipitation. For these recharge velocities, the depth of water flow needed to achieve the maximum observed temperatures would range from 800 to 1000 m. The Saline and Last Chance Ranges to the north and east respectively (Figure 1) constitute more than sufficient area for recharge. The ground water may also absorb a substantial amount of heat in lateral movement to the hot storage "reservoir." Unfortunately, no heat-flow measurements are available to the north or east of the hot spring due to the inaccessibility caused by terrain. Such data would provide useful information on the extent of the system, location of recharge area, and subsurface ground water flow (Lachenbruch and others, 1976).

For the Palm Spring system we have selected the flow to be forced by the configuration of fractures and permeable formations and by a regional piezometric gradient controlled by precipitation and elevation. If the flow of the spring results from the instability of ground water heated from below in a

permeable layer, we would expect an aspect ratio of unity for circulating cells (Sorey, 1975). This should result in heat-flow anomalies that change sign over lateral distances of the order of the depth of circulation. To achieve the maximum observed temperatures at Palm Spring, one need only circulate water down to 1 km, thus we would expect circulatory cells of 1 km across with corresponding heat-flow anomalies also 1 km across. No such heat-flow anomalies are observed in the boreholes across Saline Valley; therefore, it is doubtful that circulatory cells are the driving mechanism for Palm Spring. Furthermore, clayey layers which serve to separate shallow aquifers within the valley fill would tend to inhibit the development of such cells.

The boreholes located in the central area of the valley floor (SVG, SVH) yield relatively low heat-flow values when compared to the boreholes located along the edges of the valley (SVD, SVE, SVI, SVJ, SVK). The two boreholes lie along a main wash that runs down the central portion of the valley, lateral ground water flow beneath the wash may partially decouple the sediments from the heat flow below. Hence, the sediments along the wash may not serve as a good thermal flux plate resulting in observed low heat flow at SVG and SVH. It is also possible that the piezometric surface within the valley declines with surface elevation and that a downward piezometric gradient exists over much of the lowland area. If this is the case, a downward ground water movement of 10 mm yr^{-1} through 1000 m of valley fill with a normal Basin and Range heat flux at the base of fill would account for the low observed heat flow. Unfortunately, no piezometric surface measurements were made in order to calculate vertical and lateral piezometric gradients. No

heat-flow values were calculated for the boreholes occupying the central depression of Saline Valley (SO5, SO6, and SO7) due to the strong influence of the shallow hydrologic system on their temperature profiles.

The remaining boreholes (SVD, SVE, SVI, SVJ, SVK) are within or somewhat below the range of 75-100 mW m^{-2} one would expect for this region of the Basin and Range heat-flow province (Sass and others, 1971; Lachenbruch and Sass, 1977, 1978). Because of the rugged topography in the region, Figure 1, an estimate of its steady-state effect based on a two-dimensional approximation of topography utilizing plane slopes (Lachenbruch, 1968) was computed. This yields a maximum topographic correction of 20% for the observed heat flow at SVI and SVK and an average of 15% for the remaining boreholes. However, the above correction would be decreased if effects due to refraction between the basement-alluvium interface were considered. The first-order effect of these two corrections would be to cancel each other out; therfore, no correction has been applied to the values listed in Table 1.

CONCLUDING REMARKS

With the exception of one borehole (SVC) drilled at Palm Spring and three boreholes (SO5, SO6, and SO7) drilled around Saline Valley dry lake, heat-flow values in the Saline Valley are within or somewhat below the range one would expect for this region of the Basin and Range heat-flow province. The lack of recent volcanism in the area and the apparently normal Basin and Range heat flow suggests that geothermal systems within the valley are stable stationary phases supported by high regional heat flow with the fluid flow governed by the configuration of fractures and permeable formations and forced by a regional piezometric gradient controlled by topography and precipitation.

Upward ground-water flow from a reasonably shallow depth of 1 km can maintain the temperatures that are observed at Palm Spring. The net heat discharge from the Palm Spring system is estimated at 2 MW based on conductive and convective heat loss. Heat transfer by moving ground water in a normal Basin and Range heat-flow environment can easily provide the observed power loss. There is no need for additional heat sources such as a cooling magma chamber. Although the Palm Spring system is the only surface geothermal manifestation in the valley, conceivably hot water may come from depth in many other places along fracture zones, only to mix with cooler ground water and leak into the alluvium before it can be discharged at the surface.

References

Grim, P. J., 1977, Geothermal energy resources of the western United States, scale 1:2,500,000: National Geophysical and Solar-Terrestrial Data Center, NOAA, Boulder, Colorado.

Kilty, K. T., Chapman, D. S., and Mase, C. W., 1979, Aspects of forced convective heat transfer in geothermal systems: Department of Energy, Division of Geothermal Energy, Contract No. EG-78-C-07-1701, University of Utah.

Jennings, C. W., 1958, Geologic map of California, Death Valley Sheet, scale 1:250,000: California Division of Mines.

Jennings, C. W., 1977, Geologic map of California, scale 1:750,000: California Division of Mines.

Lachenbruch, A. H., 1968, The effect of two-dimensional topography on superficial thermal gradients: U.S. Geological Survey Bulletin 1203-E.

Lachenbruch, A. H., Sorey, M. L., Lewis, R. E., and Sass, J. H., 1976, The near-surface hydrothermal regime of Long Valley caldera: Journal of Geophysical Research, v. 81, p. 763-768.

Lachenbruch, A. H., and Sass, J. H., 1977, Heat flow in the United States and the thermal regime of the crust, in The Earth's Crust, edited by J. G. Heacock: American Geophysical Union Geophysical Monograph 20, p. 626-675.

Lachenbruch, A. H., and Sass, J. H., 1978, Models of an extending lithosphere and heat flow in the Basin and Range province: Geological Society of America Memoir 152, p. 209-250.

Olmsted, F. H., Glancy, P. A., Harrill, J. R., Rush, F. E., and Van Denburgh, A. S., 1975, Preliminary hydrogeologic appraisal of selected hydrothermal systems in northern and central Nevada: U.S. Geological Survey Open-File Report 75-56.

Renner, J. L., White, D. E., and Williams, D. L., 1975, Hydrothermal convection systems, in Assessment of geothermal resources of the United States, 1975, edited by D. E. White and D. L. Williams: U.S. Geological Survey Circular 726, p. 5-57.

Ross, D. C., 1967, Generalized geologic map of the Inyo Mountains region, California: U.S. Geological Survey Map I-506.

Ross, D. C., 1969, Descriptive petrography of three large granitic bodies in the Inyo Mountains, California: U.S. Geological Survey Professional Paper 601.

Ross, D. C., 1970, Pegmatite trachyandesite plugs and associated volcanic rocks in the Saline Range - Inyo Mountains, California: U.S. Geological Survey Professional Paper 614-D.

Sass, J. H., Lachenbruch, A. H., and Munroe, R. J., 1971a, Thermal conductivity of rocks from measurements on fragments and its application to heat-flow determinations: Journal of Geophysical Research, v. 76, p. 3391-3401.

Sass, J. H., Lachenbruch, A. H., Munroe, R. J., Greene, G. W., and Moses, T. H., Jr., 1971b, Heat flow in the western United States: Journal of Geophysical Research, v. 76, p. 6376-6413.

Sass, J. H., Ziagos, J. P., Wollenberg, H. A., Munroe, R. J., di Somma, D. E., and Lachenbruch, A. H., 1977, Application of heat-flow techniques to geothermal energy exploration, Leach Hot Springs area, Grass Valley, Nevada: U.S. Geological Survey Open-File Report 76-762.

Sass, J. H., Zoback, M. L., and Galanis, S. P., Jr., 1979, Heat flow in relation to hydrothermal activity in the southern Black Rock Desert, Nevada: U.S. Geological Survey Open-File Report, in preparation.

Sorey, M. L., 1975, Numerical modeling of liquid geothermal systems: U.S. Geological Survey Open-File Report 75-613.

Von Herzen, R. P., and Maxwell, A. E., 1959, The measurement of thermal conductivity of deep-sea sediments by a needle probe method: Journal of Geophysical Research, v. 64, p. 1557-1563.

Ward, S. H., Parry, W. T., Nash, W. P., Sill, W. R., Cook, K. L., Smith, R. B., Chapman, D. S., Brown, F. H., Whelan, J. A., and Bowman, J. R., 1978, A summary of the geology, geochemistry, and geophysics of the Roosevelt Hot Springs thermal area, Utah: Geophysics, v. 43, no. 7, p. 1515-1542.

Waring, G. A., 1965, Thermal springs of the United States and other countries of the world: U.S. Geological Survey Professional Paper 492.

APPENDIX 1

Temperature Measurements

Temperature measurements were made in boreholes of 40 to 240 m depths drilled using conventional mud-rotary techniques. With the exception of one hole, SVK, well completion involved lowering 3.2 cm I.D. steel pipe to within a meter of bottom, then pumping about 0.7 m^3 of cement-bentonite grout through the pipe, followed by a wiping plug and clear water. This amount of grout was usually sufficient to seal off the lowermost 30 to 50 m of the annulus around the pipe in these 15 cm nominal diameter holes. An additional $\sim$3 m cement plug was emplaced at the top of the well after the remainder of the hole had been backfilled with cuttings. After completion, the steel pipe was then filled with water and allowed to equilibrate to facilitate temperature measurements (better heat transfer between measuring probe and surrounding rock). Chip samples were collected from the mud flow line at 6 m intervals in all holes with the exception of SVK. Two core runs were made on boreholes SVD, SVE, SVG, SVH, and SVI comprising of one run made at an intermediate depth ($\sim$80 m) with a second near the bottom of the borehole ($\sim$140 m).

Temperatures were measured repeatedly to $\pm$ a few millidegrees at 1.52 m intervals until all transient disturbances resulting from drilling had vanished. A final equilibrium was then taken of the hole. Measurements were made on a portable four-wire thermistor probe, with resistance across the thermistor measured to a precision of 1Ω with a portable digital multimeter. Resistances were then converted to temperatures for 10°C overlapping segments based on

calibration curve of the following form:

$$T = A/(\log R+B) - C$$

Where R is resistance, T is temperature, and A, B, and C are calibration constants. Uncertainties in temperature measurements due to thermistor drift and calibration errors were determined to be negligible. Reproducibility of these types of measurements are typically to within .01°C. Temperature data along with the geothermal gradient are shown for each borehole in Figures 3 through 13.

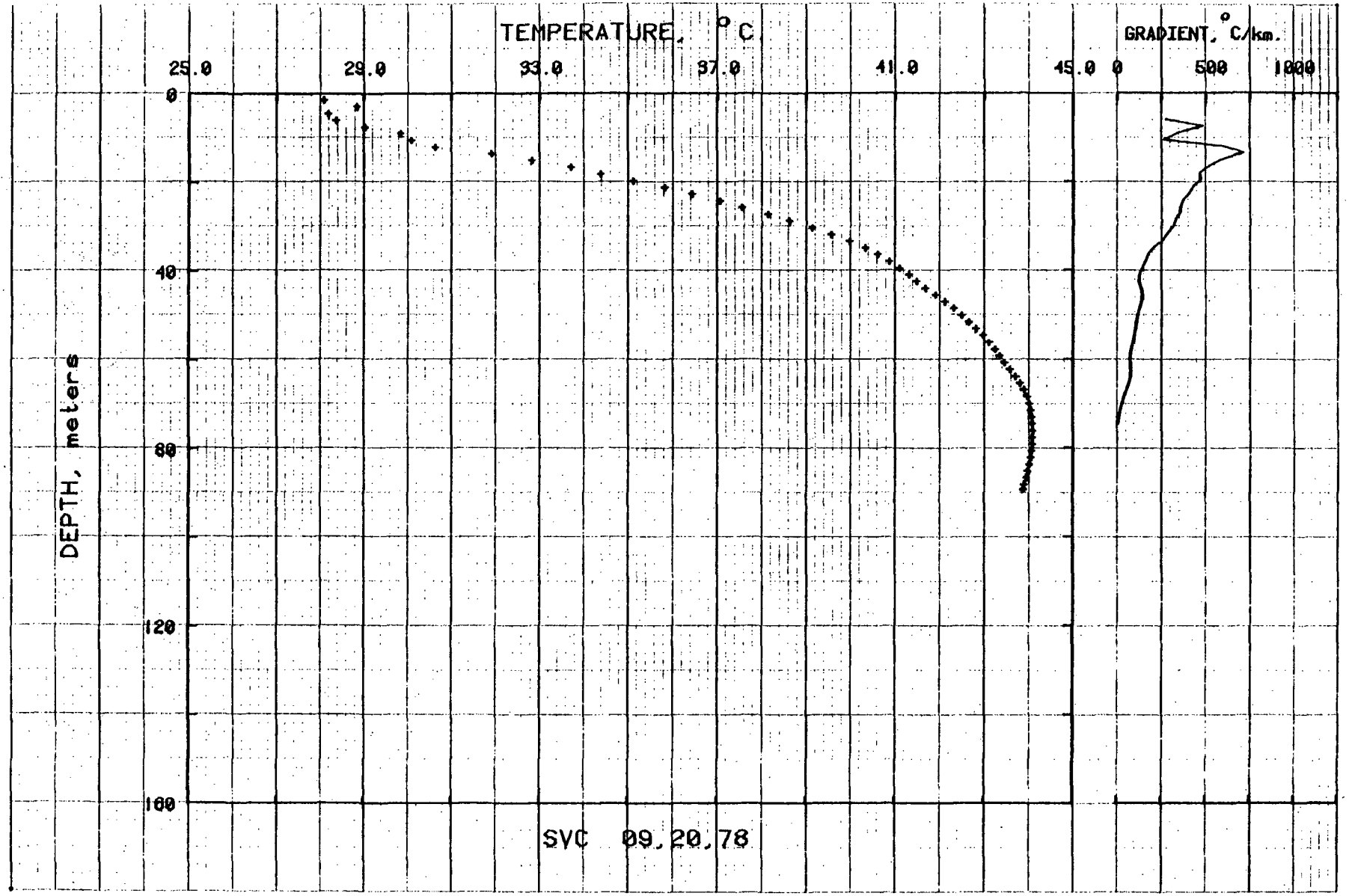

Figure 3. Temperatures and gradients for borehole SVC. Drilled July 11, 1978.

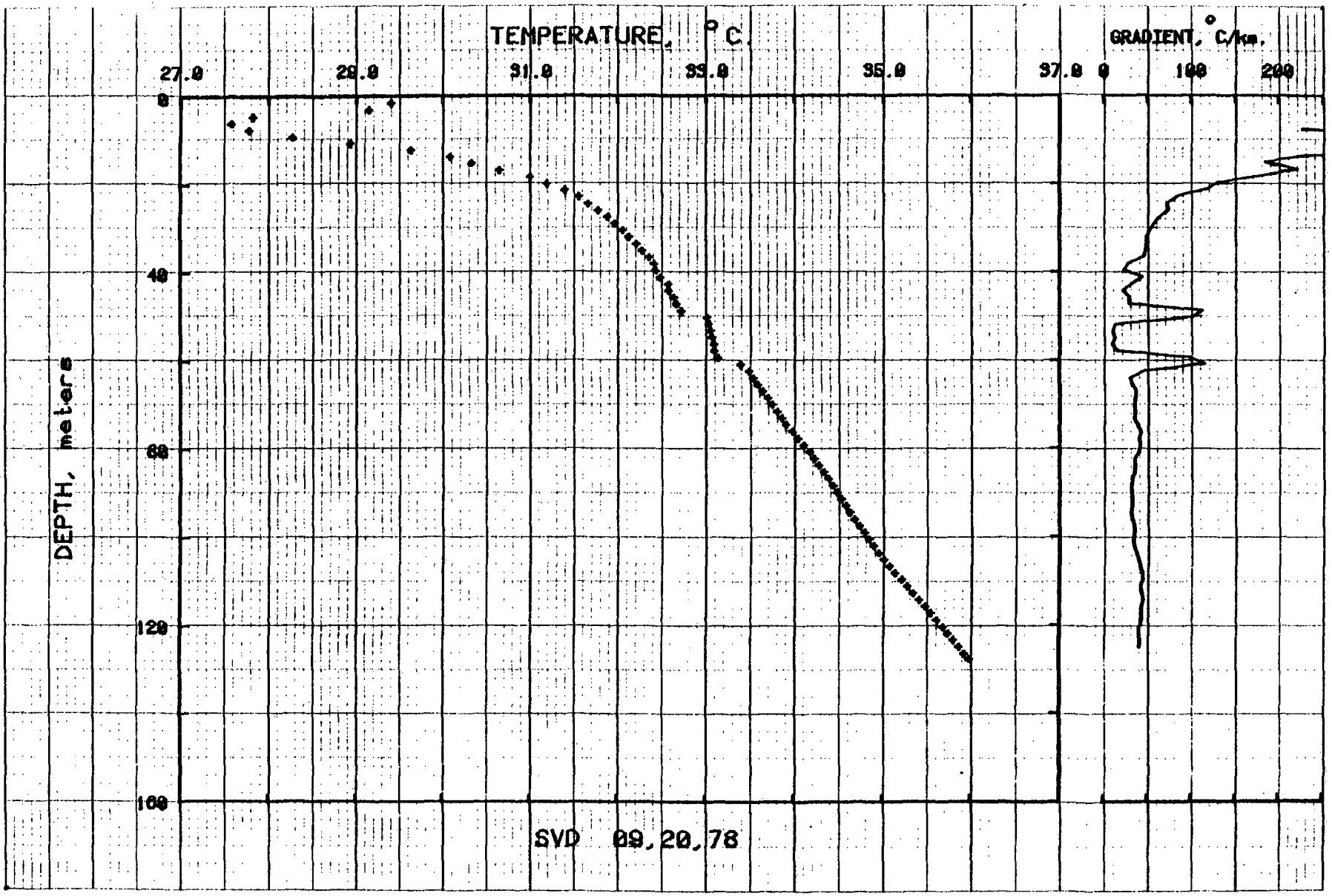

Figure 4. Temperatures and gradients for borehole SVD. Drilled July 4, 1978.

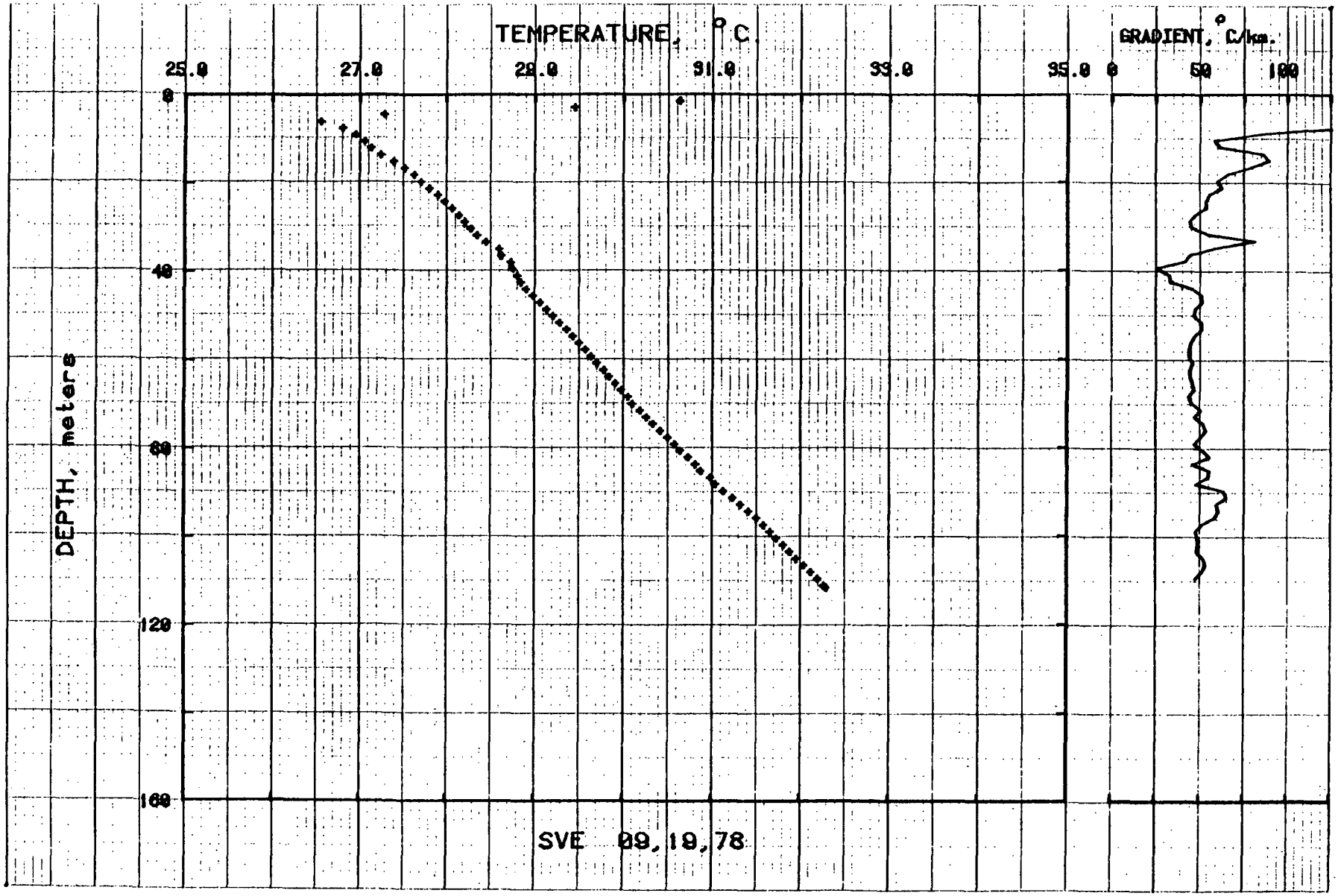

Figure 5. Temperatures and gradients for borehole SVE. Drilled July 13, 1978.

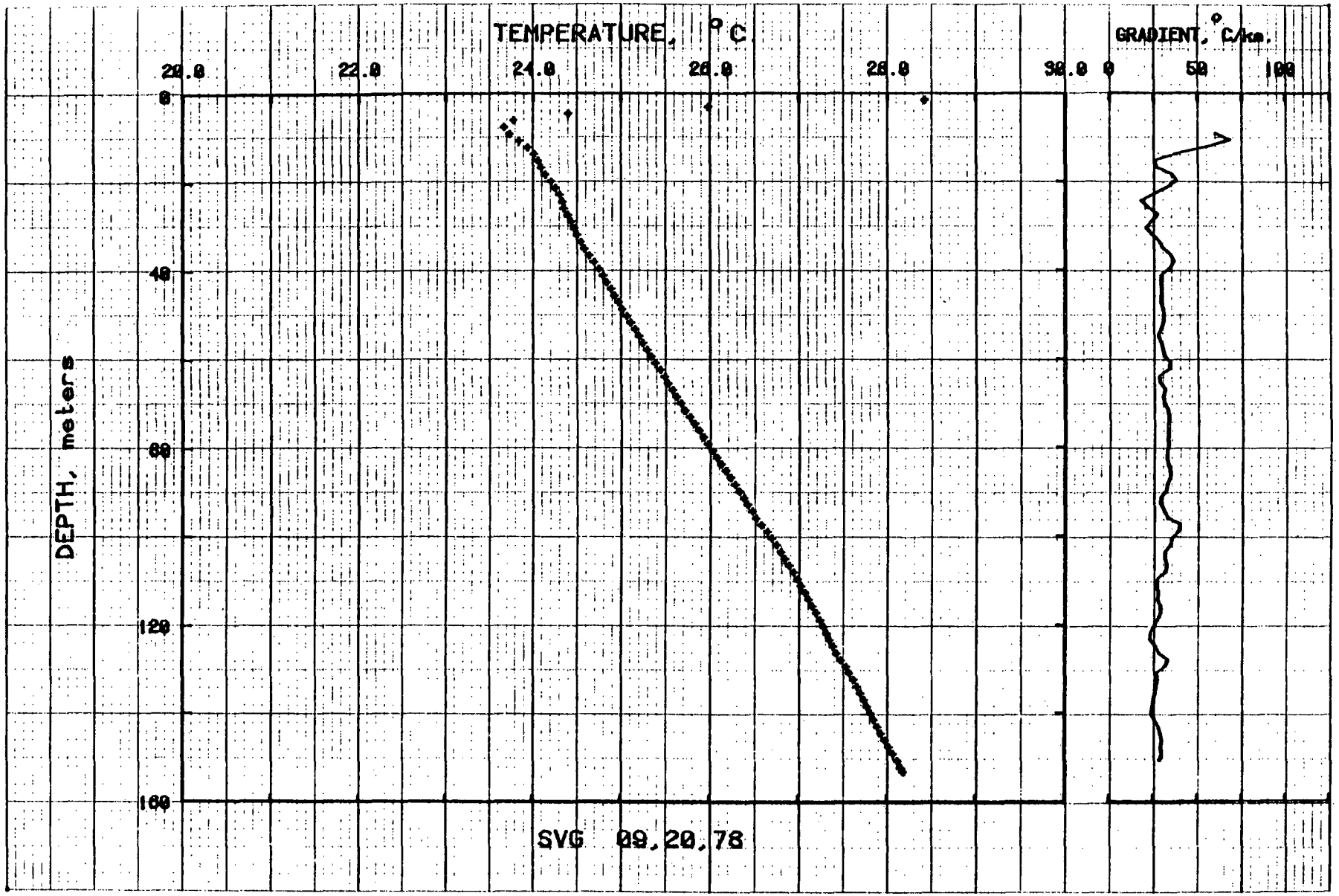

Figure 6. Temperatures and gradients for borehole SVG. Drilled July 15, 1978.

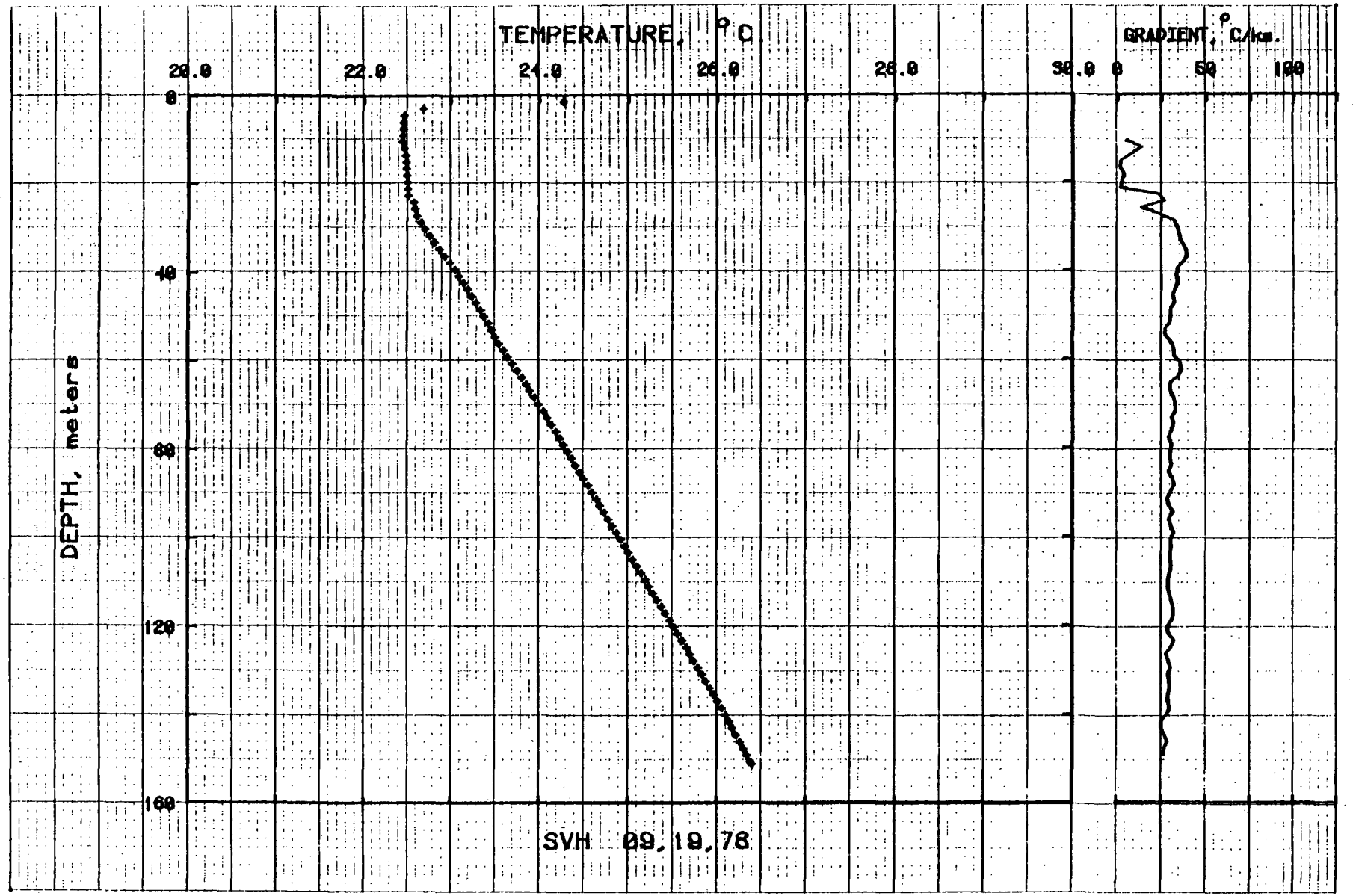

Figure 7. Temperatures and gradients for borehole SVH. Drilled July 17, 1978.

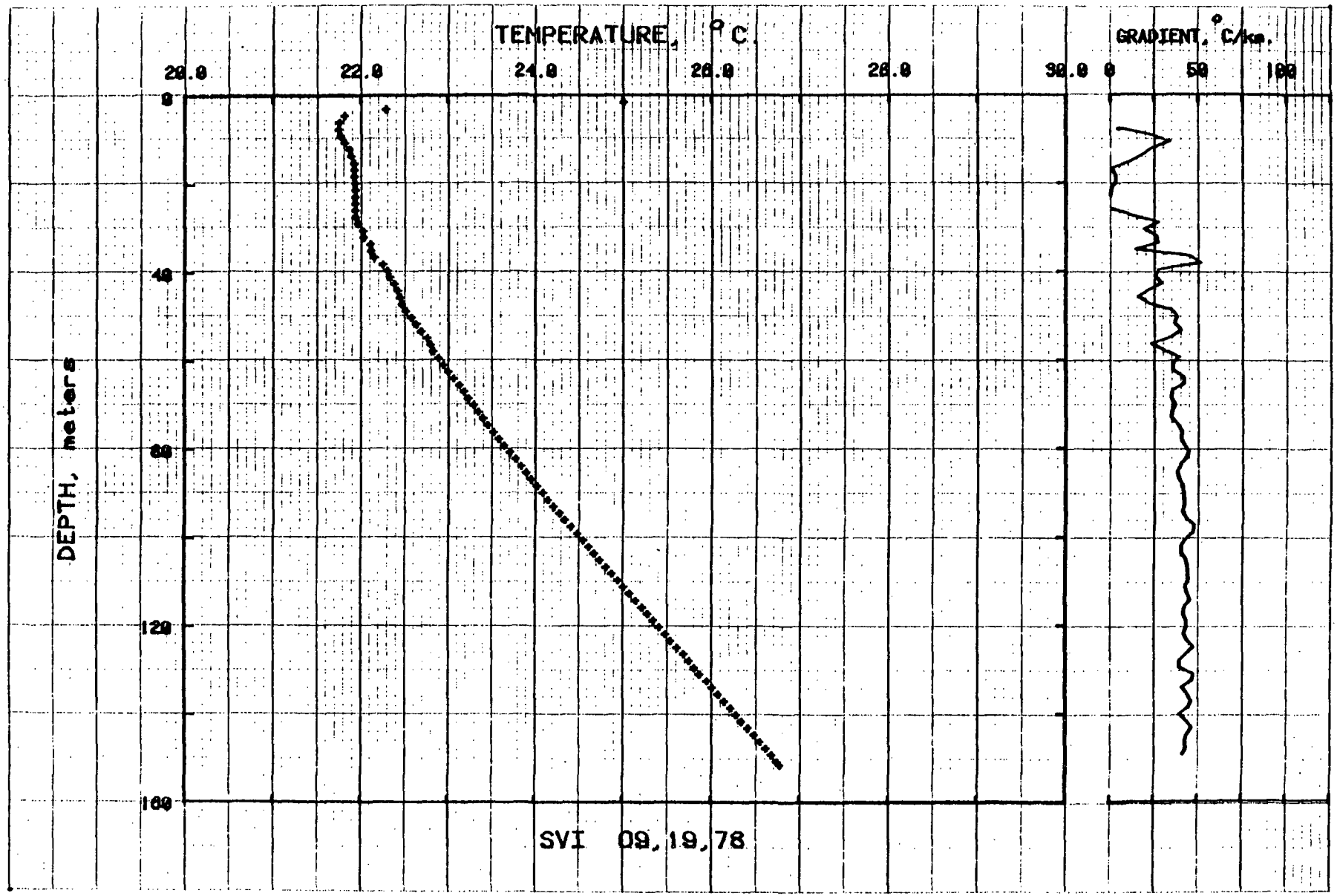

Figure 8. Temperatures and gradients for borehole SVI. Drilled July 16, 1978.

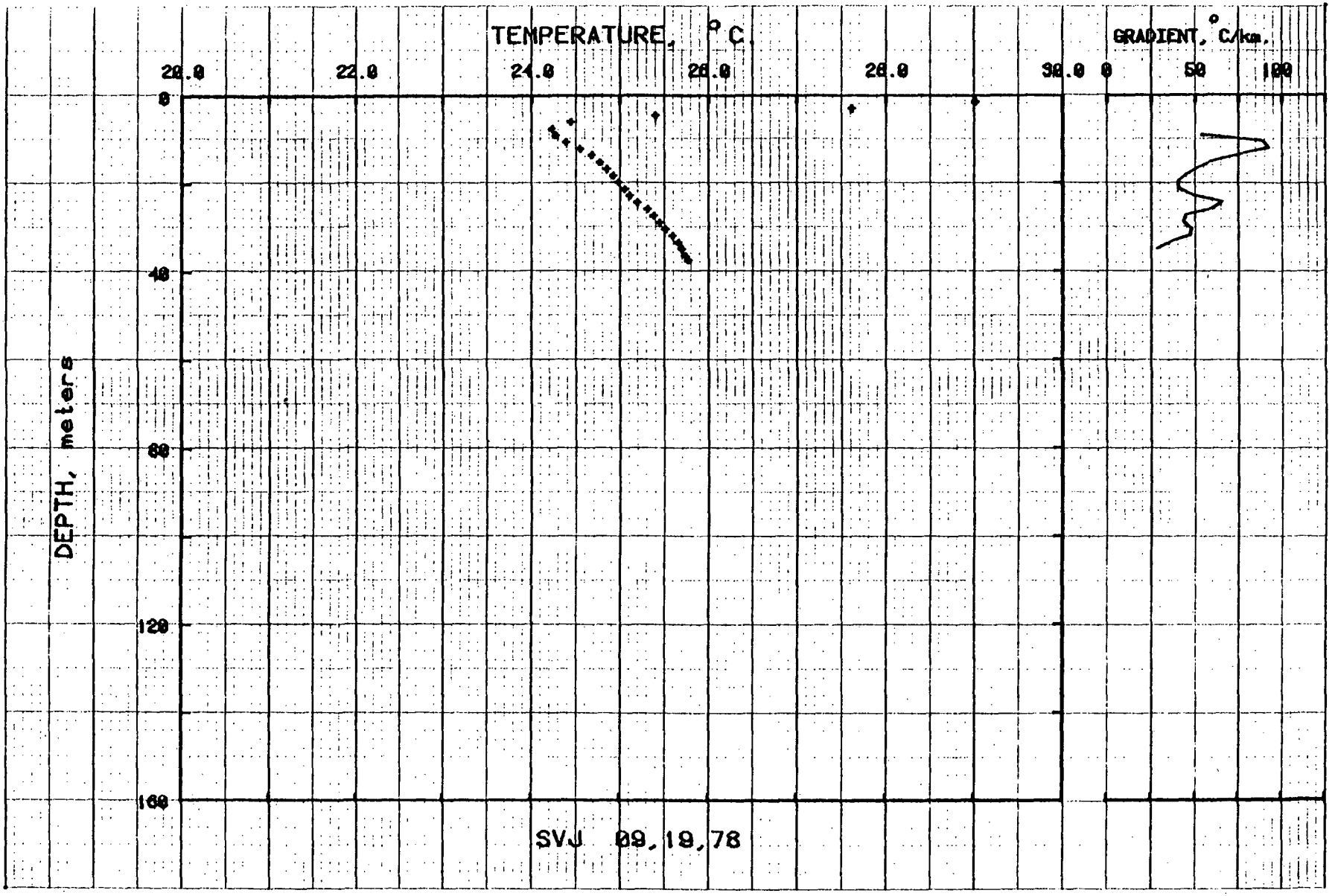

Figure 9. Temperatures and gradients for borehole SVJ. Drilled July 19, 1978.

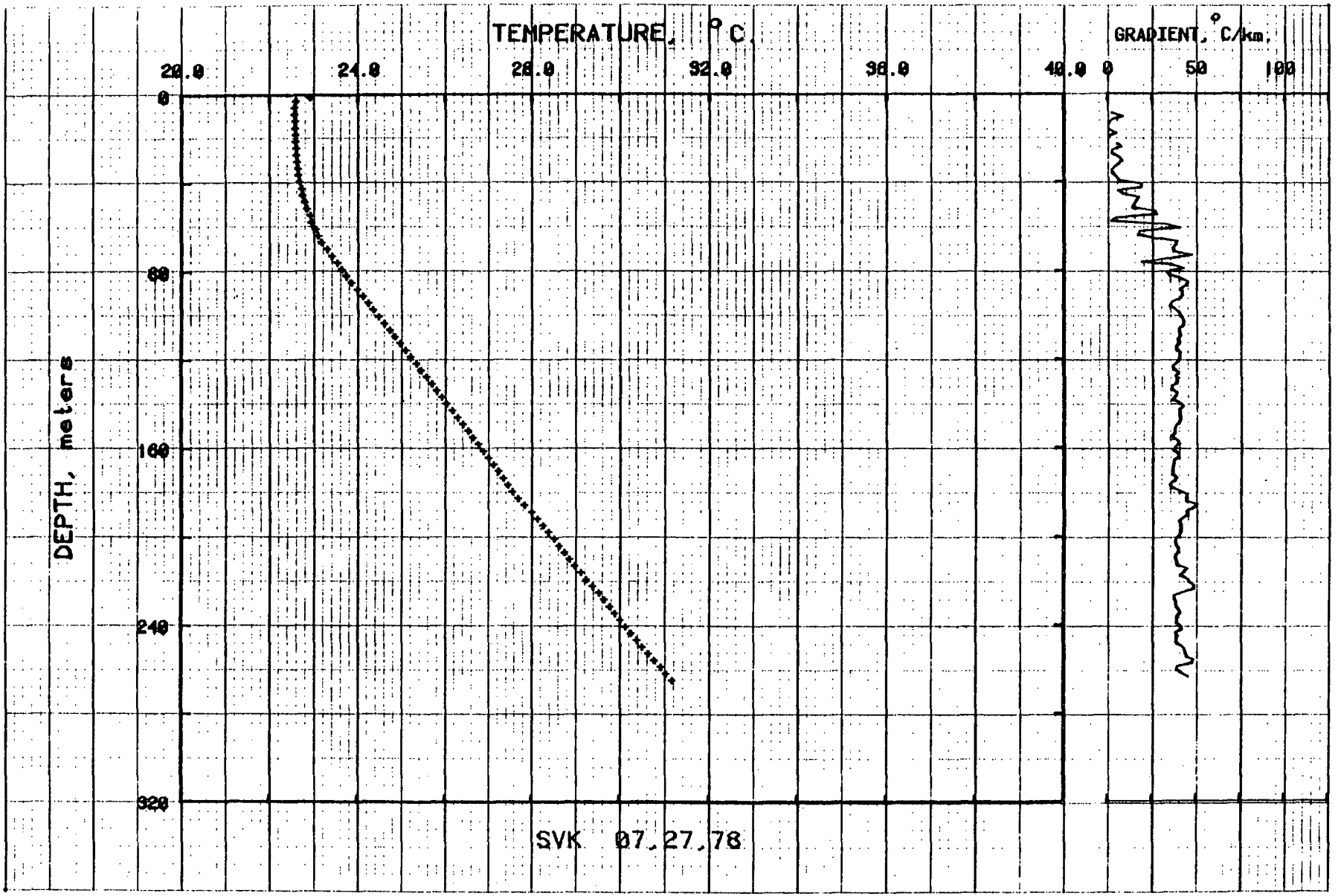

Figure 10. Temperatures and gradients for borehole SVK.

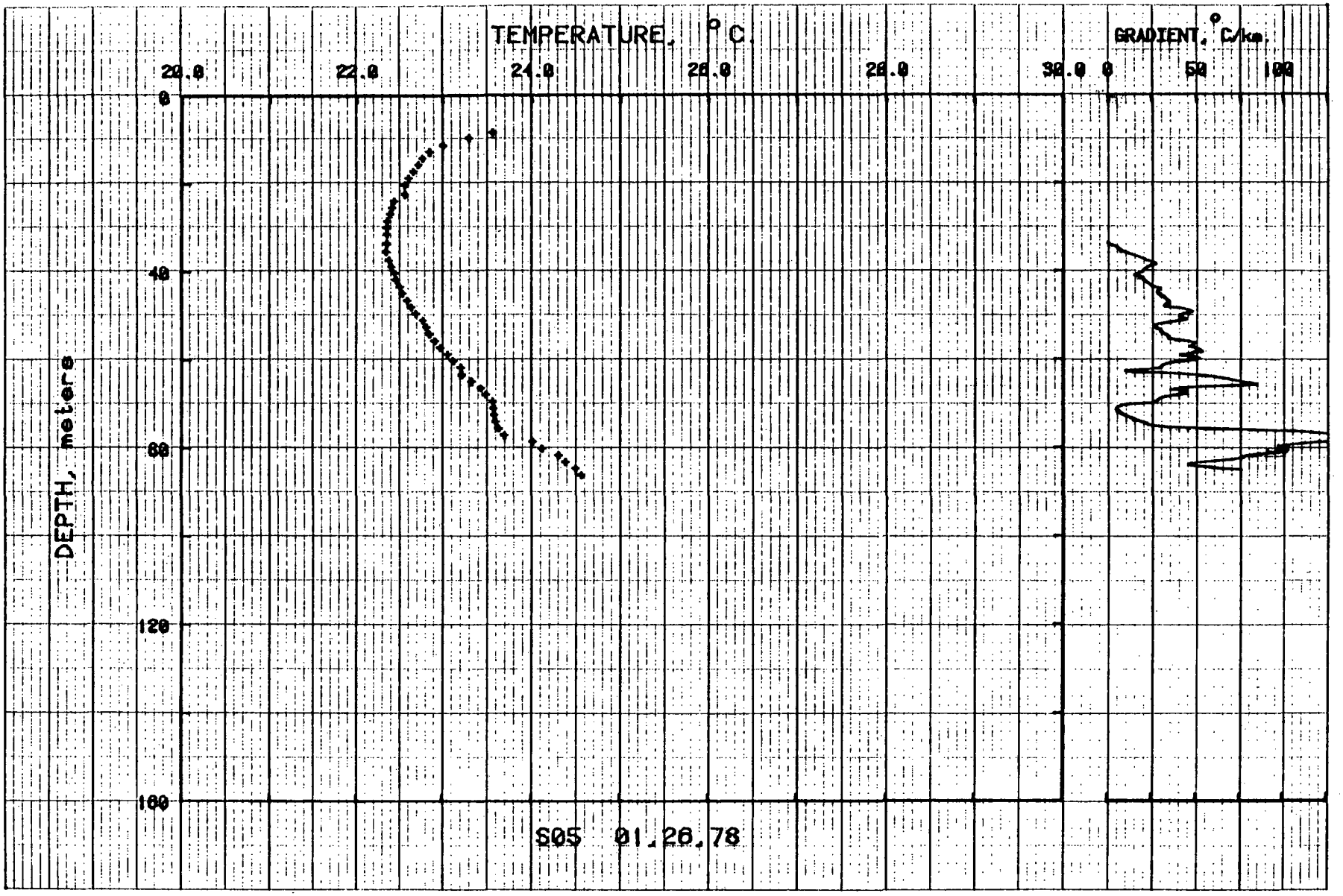

Figure 11. Temperatures and gradients for borehole S05.

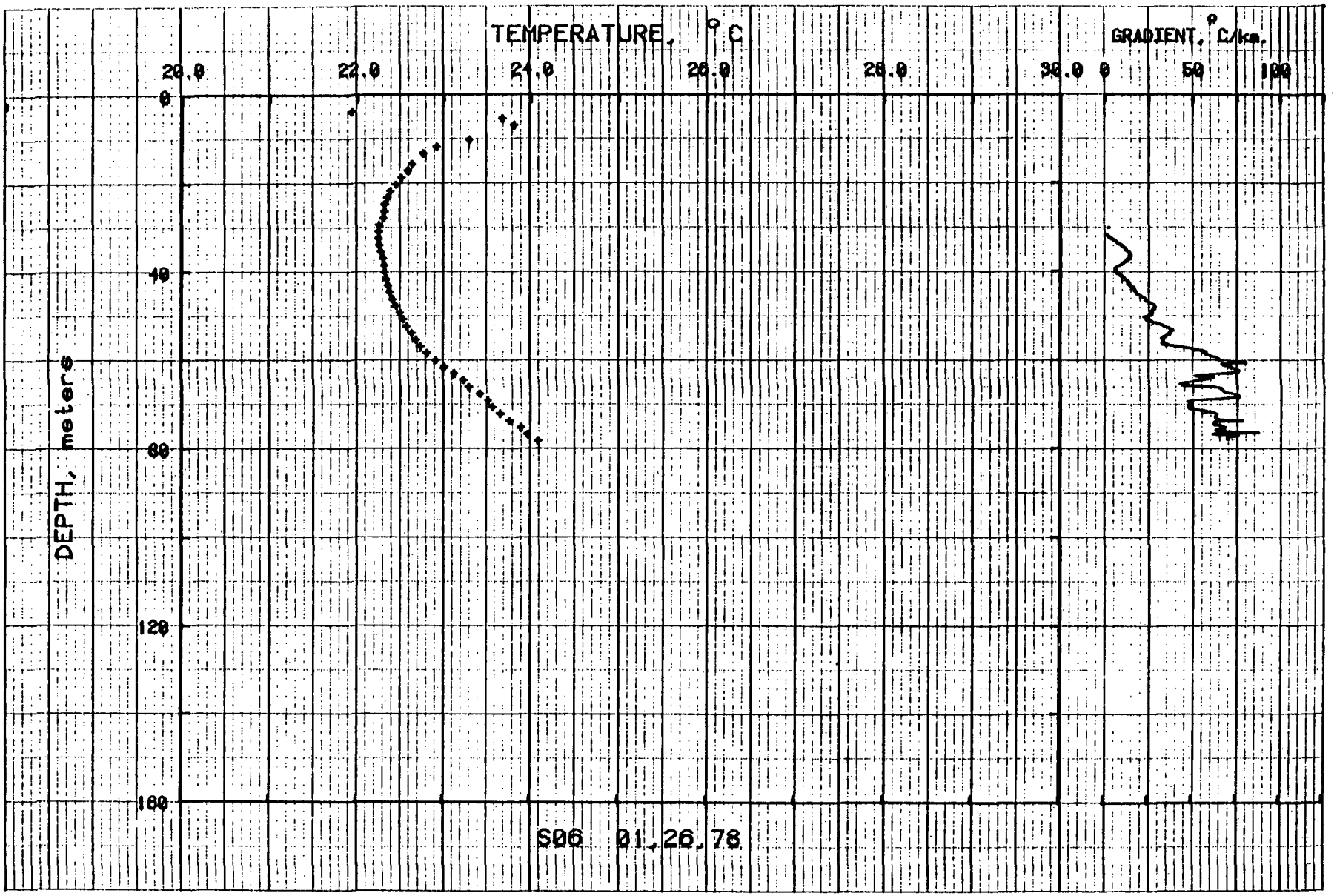

Figure 12. Temperatures and gradients for borehole S06.

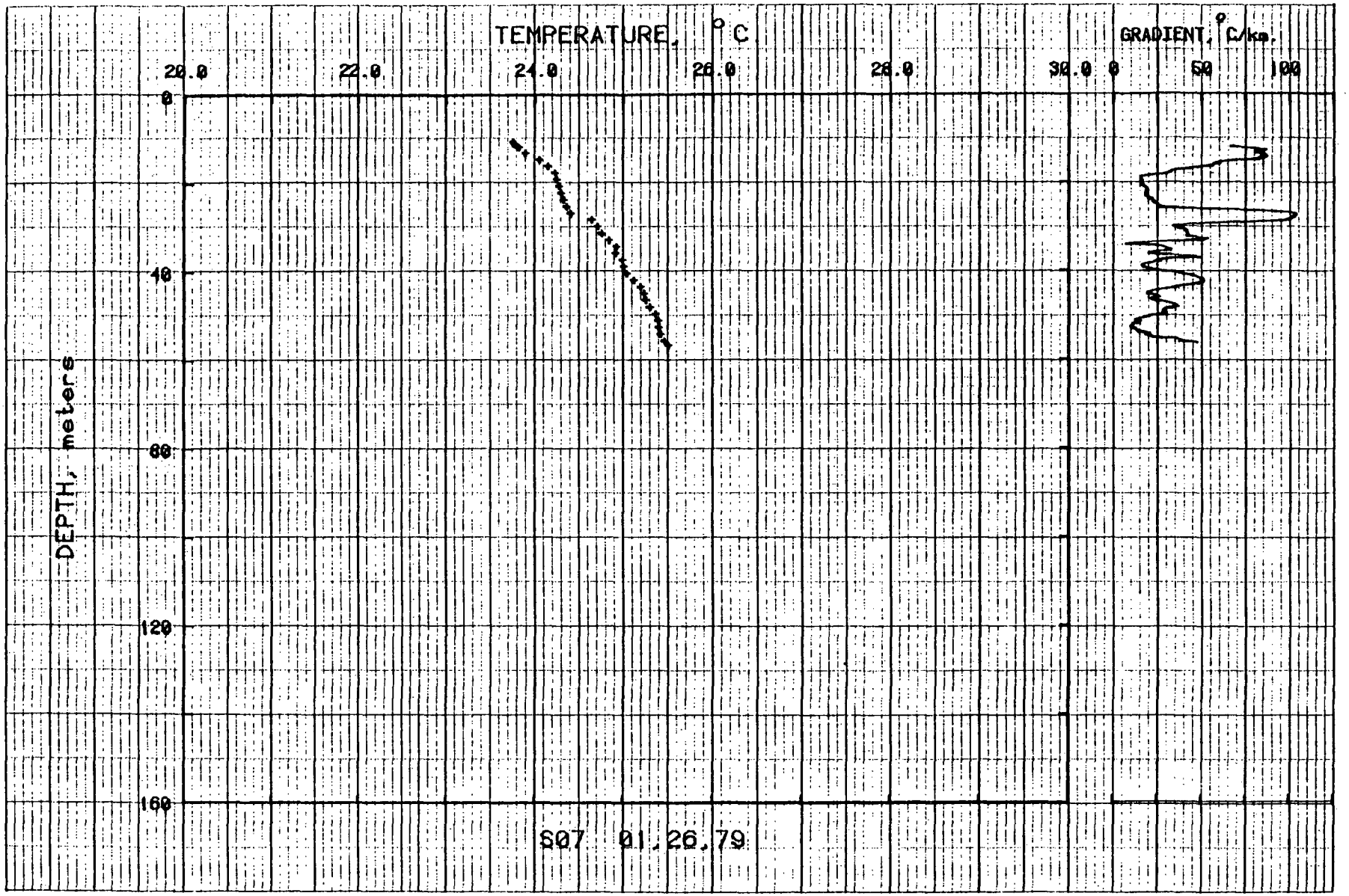

Figure 13. Temperatures and gradients for borehole S07.

APPENDIX 2

Thermal Conductivities

Two different methods were used to measure thermal conductivity of the drill samples. Conductivity measurements for the core were determined with a variant of the needle-probe method (Von Herzen and Maxwell, 1959). Thermal conductivities of chip samples were determined using the method described by Sass and others (1971a, 1971b). To determine the formation or in situ conductivity (K_f) the measured solid component conductivity (K_s) must be combined with estimates of formation porosity. The simplest model generally used is the geometric mean

$$K_f = K_s^{(1-\phi)} \cdot K_w^{\phi} \tag{1}$$

where ϕ is the fractional porosity and K_w is the conductivity of water.

An estimation of formation porosity was made utilizing K_f and K_s as measured from available core and then calculating ϕ based on the geometric mean model

$$\phi = \frac{\log \frac{(K_f/K_s)}{(K_w/K_s)}}{} \tag{2}$$

where K_f and K_s were determined via needle probe and chip method respectively. Porosity measurements were also made on different sections of all suitable core that had not disintegrated or dried out. A comparison of the results, Table 2, shows reasonably good agreement between the two methods and yields

an average porosity for the valley fill of 28%, excluding SVC. SVC is close to the hot spring and its low porosity may be due to the cementing action of hot spring waters. This inference is supported by the large amount of tufaceous material found in the drill cuttings and by the temperature-depth plot of SVC which indicates a convecting hydrothermal system.

Due to the heterogeneity and poor sorting of valley fill, the porosity may be expected to vary rapidly with depth and/or location. The core represents intervals where the rock was coherent enough such that core was recoverable; therefore, the cores obtained and porosities measured may not be an adequate sample of the valley fill. Such intervals may have a lower porosity than intervals where core was not recoverable due to the presence of sand or gravels, thereby biasing our measured porosities lower than the average in situ porosity.

Based on the foregoing discussion and the porosity results summarized in Table 2, formation conductivity, K_f, was calculated from the solid component conductivity using an average porosity of 30% and the geometric mean model of equation 1. A conservative estimate of the error in ϕ ($\pm$5%) was used to estimate the error in the computed formation conductivity and heat flow, but it leaves unanswered the question of whether or not large systematic errors were introduced because the porosities measured on cores may not adequately represent the average porosity of valley fill.

TABLE 2. Saline Valley porosity calculations

Hole	Depth m	K_s W m^{-1} $°K^{-1}$	K_f W m^{-1} $°K^{-1}$	ϕ_c* %	ϕ_m** %
SVC	80	2.16	1.72	18	13
SVD	80	2.91	1.86	29	24
SVG	80	2.76	1.82	28	37
	140				23
SVH	80	3.00	1.76	34	
	140	2.66	1.69	31	26
SVI	80	2.72	1.87	25	
	140	2.77	1.71	32	23

*ϕ_c, porosity calculated for cores from K_f and K_s utilizing a geometric mean model (equation 2).

**ϕ_m, apparent porosity [(wet weight - dry weight)/(wet weight) x 100] as measured from core.

TABLE 3. Thermal conductivities for SVC

Depth range m	ft	K_s W m^{-1} $°K^{-1}$	K_s mcal cm^{-1} sec^{-1} $°C^{-1}$	ϕ_{corr} %	K_f W m^{-1} $°K^{-1}$	K_f mcal cm^{-1} sec^{-1} $°C^{-1}$
26-32	85-105	2.61	6.22	18	2.00	4.79
38-44	125-145	2.49	5.95	18	1.93	4.61
62-69	205-225	2.40	5.74	18	1.87	4.47
75-81	245-265	2.16	5.17	18	1.72	4.10
87-93	285-305	2.24	5.36	18	1.77	4.23
79-80	258-264	(needle probe)			1.72	4.11

TABLE 4. Thermal conductivities for SVD

Depth range m	Depth range ft	K_s W m^{-1} $°K^{-1}$	K_s mcal cm^{-1} sec^{-1} $°C^{-1}$	ϕ_{corr} %	K_f W m^{-1} $°K^{-1}$	K_f mcal cm^{-1} sec^{-1} $°C^{-1}$
24-30	80-100	2.24	5.35	30	1.51	3.61
37-43	120-140	1.91	4.55	30	1.35	3.23
49-55	160-180	2.83	6.75	30	1.78	4.25
61-67	200-220	2.98	7.13	30	1.85	4.41
73-79	240-260	2.91	6.94	30	1.81	4.33
85-91	280-300	2.84	6.78	30	1.78	4.26
98-104	320-340	2.88	6.87	30	1.80	4.30
110-116	360-380	3.08	7.35	30	1.89	4.51
127-128	418-420	2.30	5.49	30	1.54	3.68
79-80	258-261	(needle probe)			1.86	4.45

TABLE 5. Thermal conductivities for SVE

Depth range m	Depth range ft	K_s W m^{-1} $°K^{-1}$	K_s mcal cm^{-1} sec^{-1} $°C^{-1}$	ϕ_{corr} %	K_f W m^{-1} $°K^{-1}$	K_f mcal cm^{-1} sec^{-1} $°C^{-1}$
24-30	80-100	2.33	5.56	30	1.55	3.71
37-43	120-140	2.55	6.09	30	1.65	3.95
49-55	160-180	2.89	6.90	30	1.81	4.31
61-67	200-220	3.30	7.87	30	1.98	4.73
73-79	240-260	3.23	7.72	30	1.95	4.66
85-91	280-300	2.73	6.52	30	1.74	4.14

TABLE 6. Thermal conductivities for SVG

Depth range m	Depth range ft	K_s W m^{-1} $°K^{-1}$	K_s mcal cm^{-1} sec^{-1} $°C^{-1}$	ϕ_{corr} %	K_f W m^{-1} $°K^{-1}$	K_f mcal cm^{-1} sec^{-1} $°C^{-1}$
26-32	85-105	2.77	6.61	30	1.75	4.19
38-44	125-145	3.07	7.33	30	1.88	4.50
50-56	165-185	2.79	6.67	30	1.76	4.21
62-69	205-225	2.86	6.83	30	1.79	4.28
75-81	245-265	2.76	6.59	30	1.75	4.18
87-93	285-305	2.30	5.49	30	1.54	3.68
99-105	325-345	2.62	6.25	30	1.69	4.03
111-117	365-385	2.46	5.89	30	1.61	3.85
122-128	400-420	2.29	5.48	30	1.53	3.67
134-140	440-460	2.68	6.39	30	1.71	4.09
146-152	480-500	2.66	6.36	30	1.70	4.07
152-154	500-504	2.72	6.51	30	1.73	4.13
78-79	257-260	(needle probe)			1.82	4.35

TABLE 7. Thermal conductivities for SVH

Depth range m	Depth range ft	K_s W m^{-1} $°K^{-1}$	K_s mcal cm^{-1} sec^{-1} $°C^{-1}$	ϕ_{corr} %	K_f W m^{-1} $°K^{-1}$	K_f mcal cm^{-1} sec^{-1} $°C^{-1}$
24-30	80-100	1.76	4.21	30	1.28	3.05
37-43	120-140	2.39	5.70	30	1.58	3.78
49-55	160-180	3.13	7.48	30	1.91	4.56
61-67	200-220	2.62	6.27	30	1.69	4.03
73-79	240-260	2.66	6.35	30	1.70	4.07
85-91	280-300	2.87	6.85	30	1.80	4.29
98-104	320-340	2.65	6.32	30	1.70	4.06
110-116	360-380	2.81	6.71	30	1.77	4.23
122-128	400-420	2.91	6.96	30	1.81	4.33
134-140	440-460	2.76	6.60	30	1.75	4.18
146-152	480-500	3.00	7.15	30	1.85	4.43
78-79	257-260	(needle probe)			1.76	4.21
139-140	457-459	(needle probe)			1.69	4.03

TABLE 8. Thermal conductivities for SVI

Depth range m	Depth range ft	K_s W m^{-1} $°K^{-1}$	K_s mcal cm^{-1} sec^{-1} $°C^{-1}$	ϕ_{corr} %	K_f W m^{-1} $°K^{-1}$	K_f mcal cm^{-1} sec^{-1} $°C^{-1}$
24-30	80-100	2.69	6.43	30	1.72	4.10
37-43	120-140	2.63	6.28	30	1.69	4.04
49-55	160-180	2.48	5.92	30	1.62	3.88
61-67	200-220	2.48	5.91	30	1.62	3.88
73-79	240-260	2.72	6.49	30	1.73	4.13
85-91	280-300	2.58	6.17	30	1.67	3.98
98-104	320-340	2.53	6.04	30	1.64	3.93
110-116	360-380	2.46	5.86	30	1.61	3.85
122-128	400-420	2.24	5.34	30	1.51	3.61
134-140	440-460	2.77	6.61	30	1.75	4.19
146-152	480-500	2.67	6.37	30	1.71	4.08
78-79	257-259	(needle probe)			1.87	4.47
139-140	457-460	(needle probe)			1.71	4.09

TABLE 9. Thermal conductivities for SVJ

Depth range m	Depth range ft	K_s W m^{-1} $°K^{-1}$	K_s mcal cm^{-1} sec^{-1} $°C^{-1}$	ϕ_{corr} %	K_f W m^{-1} $°K^{-1}$	K_f mcal cm^{-1} sec^{-1} $°C^{-1}$
26-32	85-105	2.36	5.62	30	1.57	3.74
38-44	125-145	2.12	5.06	30	1.45	3.47

APPENDIX 3

Lithologic Descriptions

The lithology of seven of the holes drilled in Saline Valley are described in Tables 10 through 16. The holes were drilled using conventional rotary-mud methods by T. Clingan (Western Geophysical Company) under the supervision of J. Porter (USGS).

Ditch samples were collected at six-meter intervals in all of the holes drilled by the USGS, and one-meter cores were taken in several of the holes (cored intervals are indicated on the charts). The samples were described in the lab after examination with a 10X hand lens.

TABLE 10. Lithology for borehole SVC.

Hole: SVC **Location:** Saline Valley

Started: 7-4-78 **Completed:** 7-11-78 **Drilled by:** Clingan

Notes by: Galanis **Scale:** 1" = 25 meters **Sheet** 1 **of** 1

Depth (meters)	Graphic column	cored interval	Rock type	
0			Calcareous tufa and silt	Hot spring and lake(?) deposits
20				
25			Gravel and silt	Fan deposit
50				
56			Calcareous tufa, silt, and gravel	Fan and reworked(?) hot spring deposits
69				
75		79 m 80 m	Gravel and silt	Fan deposit
93 T.D.				

TABLE 11. Lithology for borehole SVD.

Hole: SVD **Location:** Saline Valley

Started: 7-1-78 **Completed:** 7-4-78 **Drilled by:** Clingan

Notes by: Galanis **Scale:** 1" = 25 meters **Sheet** 1 **of** 1

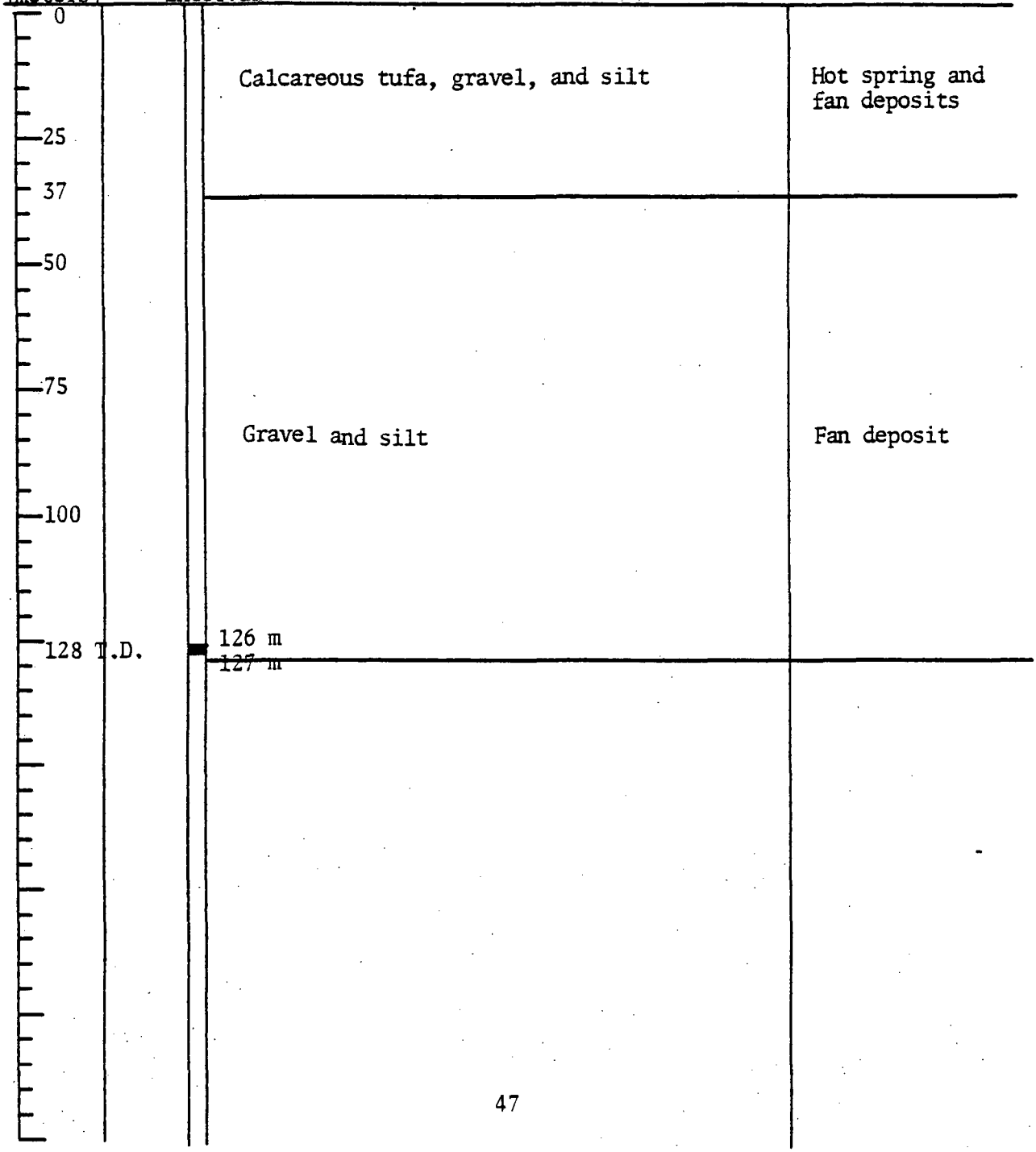

TABLE 12. Lithology for borehole SVE.

Hole: SVE **Location:** Saline Valley

Started: 7-12-78 **Completed:** 7-13-78 **Drilled by:** Clingan

Notes by: Galanis **Scale:** 1" = 25 meters **Sheet** 1 **of** 1

Depth (meters)	Graphic column	Rock type	
0		Gravel and silt	Fan deposit
18		Calcareous tufa, gravel, and silt	Fan and reworked(?) hot spring deposits
43		Gravel and silt	Fan deposit
50			
75			
100			
116 T.D.			

TABLE 13. Lithology for borehole SVG.

Hole: SVG **Location:** Saline Valley

Started: 7-14-78 **Completed:** 7-15-78 **Drilled by:** Clingan

Notes by: Galanis **Scale:** 1" = 25 meters **Sheet** 1 **of** 1

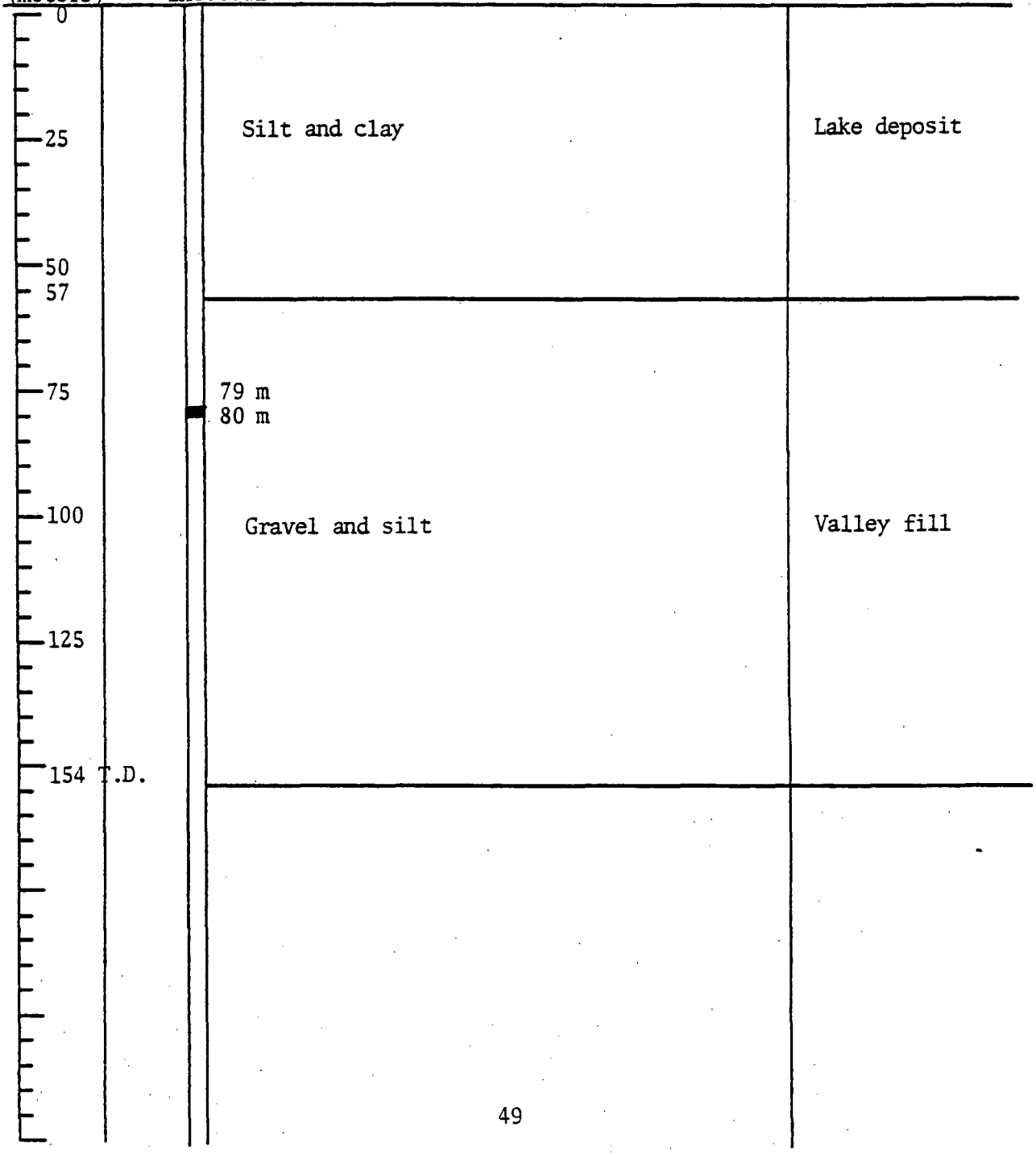

TABLE 14. Lithology for borehole SVH.

Hole: SVH **Location:** Saline Valley

Started: 7-15-78 **Completed:** 7-16-78 **Drilled by:** Clingan

Notes by: Galanis **Scale:** 1" = 25 meters **Sheet** 1 **of** 1

Depth (meters)	Graphic column	Rock type	
0			
25		Silt and clay	Lake deposit
50			
55			
75			
100		Gravel and silt	Valley fill
125			
152 T.D.			

TABLE 15. Lithology for borehole SVI.

Hole: SVI **Location:** Saline Valley

Started: 7-17-78 **Completed:** 7-17-78 **Drilled by:** Clingan

Notes by: Galanis **Scale:** 1" = 25 meters **Sheet** 1 **of** 1

Depth (meters)	Graphic column	cored interval	Rock type	
0				
25			Silt and clay	Lake deposit
50				
55				
75				
100			Gravel and silt	Valley fill
125				
		140 m 141 m		
152 T.D.				

TABLE 16. Lithology for borehole SVJ.

Hole: SVJ **Location:** Saline Valley

Started: 7-18-78 **Completed:** 7-19-78 **Drilled by:** Clingan

Notes by: Galanis **Scale:** 1" = 25 meters **Sheet** 1 **of** 1

Depth (meters)	Graphic column	Rock type	
0		Gravel and silt	Fan deposit
25			
44 T.D.			